Cost-effective, Thin-film SOFCs for Reliable Power Generation

UNIVERSITY OF SOUTH CAROLINA

PI: Fanglin (Frank) Chen

Co-PIs: Kevin Huang (University of South Carolina)
Greg Tao (Chemtronergy LLC)

Project Overview

- **Project Title**: Cost-effective, Thin-film SOFCs for Reliable Power Generation
- **Award No**: DE-FE0031670
- **Project Period**: 8/17/2018—8/16/2020
- **Project Manager**: Dr. Venkat Venkataraman

UNIVERSITY OF SOUTH CAROLINA

Fanglin (Frank) Chen (PI)

Kevin Huang (Co-PI)

Chemtronergy LLC

Greg Tao

Project Overview

Objective:

The overall objective of the proposed work is to develop an advanced SOFC technology that cost-effectively and reliably generates electricity for distributed and central generation applications. The proposed innovative technology will be built-on a planar metal-supported SOFC (MS-SOFC) through a cost-effective phase-inversion tape-casting and APS-based manufacturing process.

Project Goals:

- Fabrication of porous metal substrates with graded porosity using a phase-inversion tape-casting process.
- Development of atmospheric plasma spray (APS) process for depositing all active layers, including anode, electrolyte and cathode, supported on a porous metal substrate.
- Characterization of the metal-supported SOFCs to achieve high performance and stability.

Outline

- ❑ Background
- ❑ Project objectives and work progress
  - ➢ Preparation and optimization of metal support
  - ➢ Preparation of metal supported SOFC(MS-SOFC)
    - Deposition of ScSZ-NiO anode
    - Deposition of ScSZ electrolyte
    - Deposition of LSCF cathode
- ❑ Summary
- ❑ Ongoing and future work
- ❑ Acknowledgements

Background – Advantages of MS-SOFC

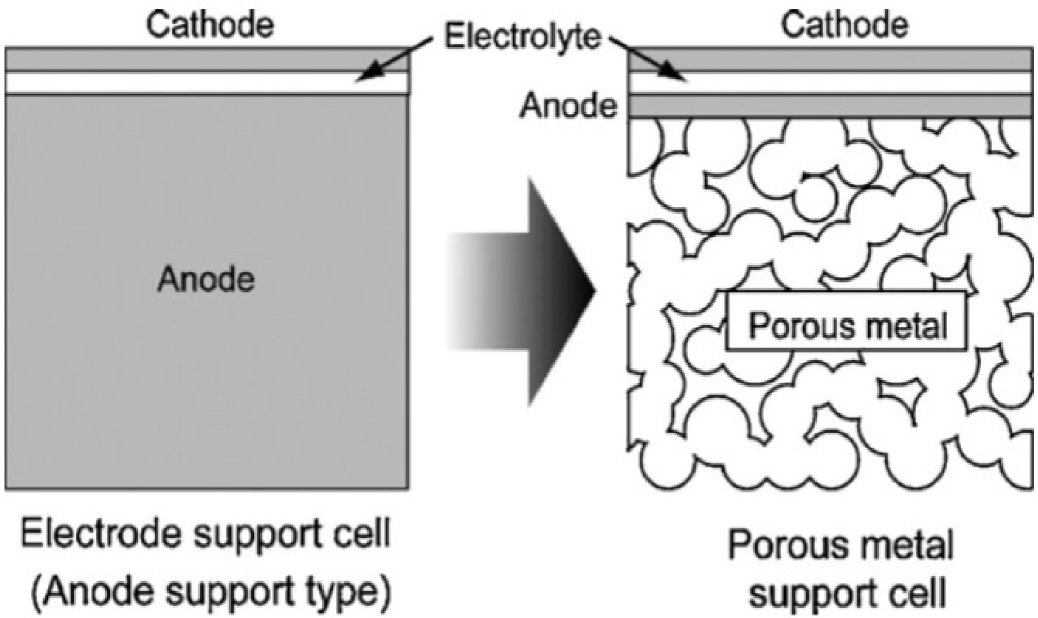

- ✓ **Low cost**
- ✓ **High strength**
- ✓ **Better workability**
- ✓ **Good thermal conductivity**
- ✓ **Quicker start-up**

Fig. 1.Schematic representation of anode-supported cell (ASC) and metal-supported cell (MSC).

J. Power Source 2010, 195, 106-109

Background – Concentration Polarization

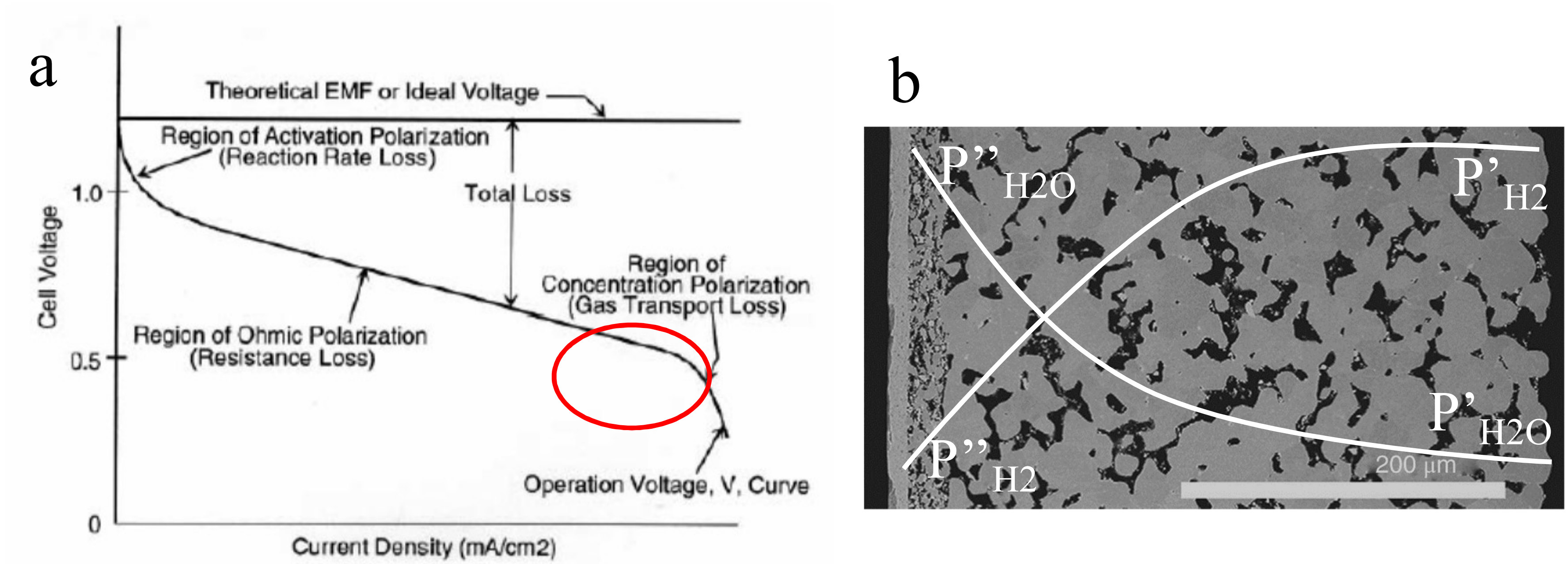

Fig.2. (a) Ideal and actual fuel cell voltage/current characteristics; (b) Schematic diagram of H_2 and H_2O diffusion in the anode substrate.

J. Power Sources 2011, 196, 7117–7125

Background – Open Porous Microstructure from Phase-Inversion Tape Casting

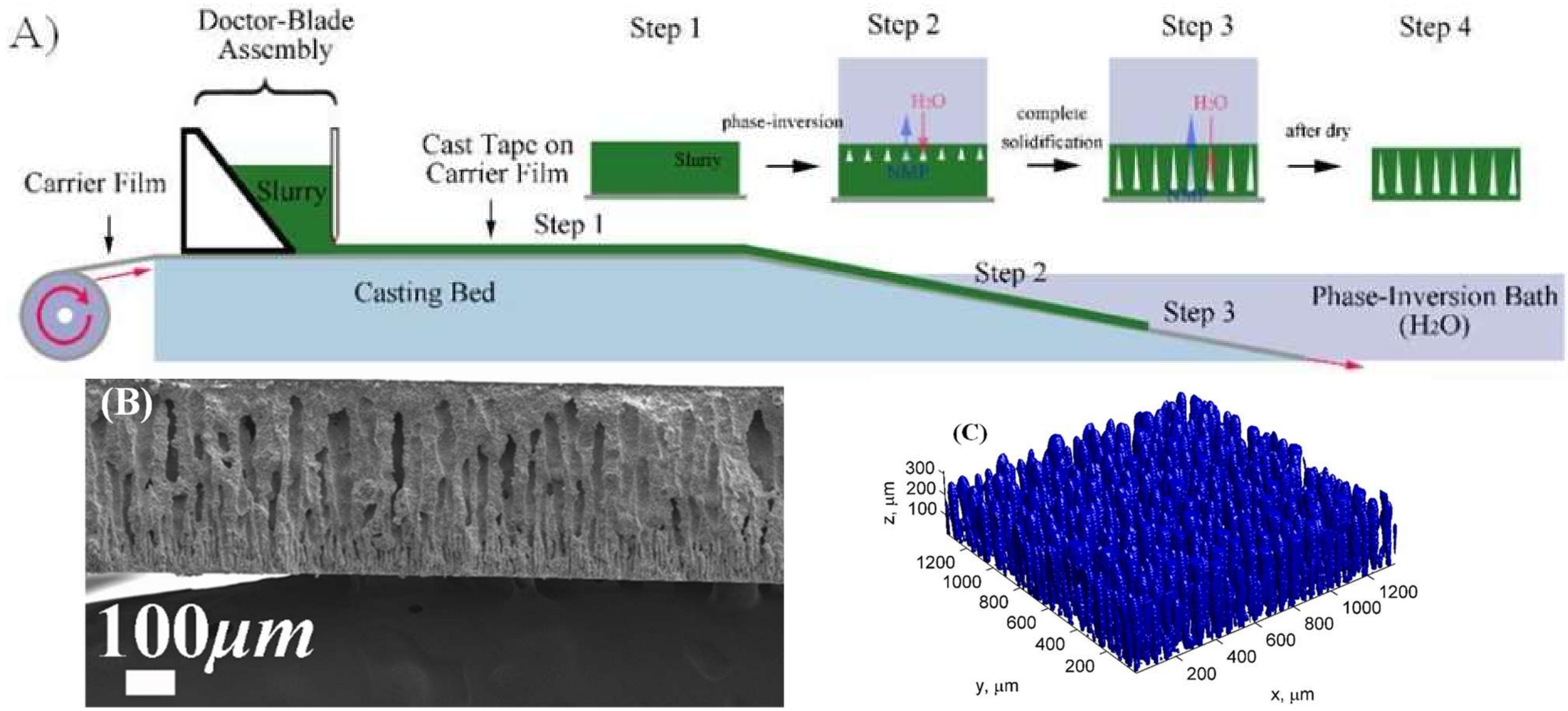

Fig. 3. A) Schematic diagram of the phase-inversion tape casting process; B) Cross-sectional SEM image of the metal support, and C) 3D X-ray computed tomography image of the porous metal support

Electrochem. Commun. 2015, 61, 106-109

Project Goal 1 – Preparation of Porous Metal Support using Phase-Inversion Tape-Casting Process

Solvent
Polymer binder
Additive
Metal powders

↓

Slurry

↓

De-airing

↓

Tape Casting

↓

Phase Inversion

↓

Drying

↓

Sintering

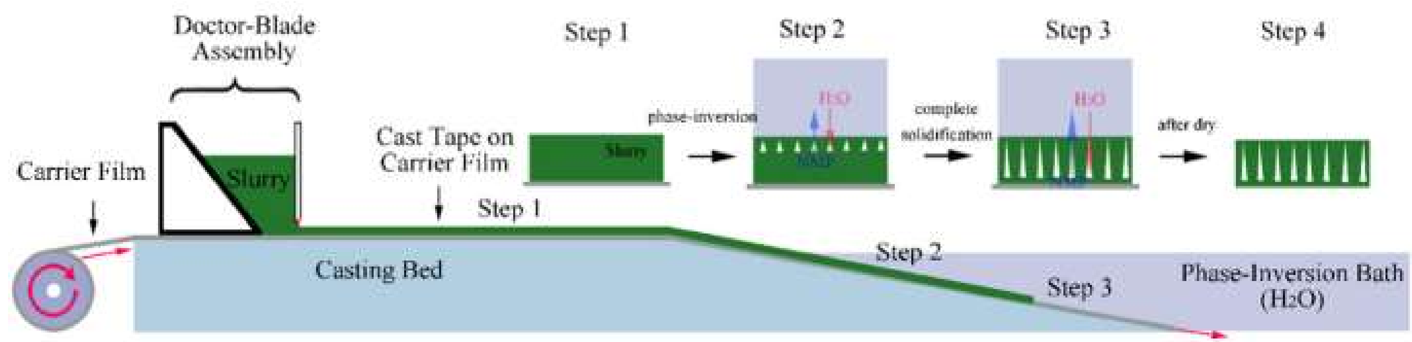

1) Tape-cast of the slurry with stainless steel (SS) powders by dissolving polyethersulfone (PES) binder and polyvinylpyrrolidone (PVP) additive in N-methyl-2-pyrrolidone (NMP) solvent
2) Immersion of the tape into non-solvent (water) bath
3) NMP leaves the tape and NMP/water exchange takes place
4) Formation of columnar metal support microstructure

Characterization of Metal Powders

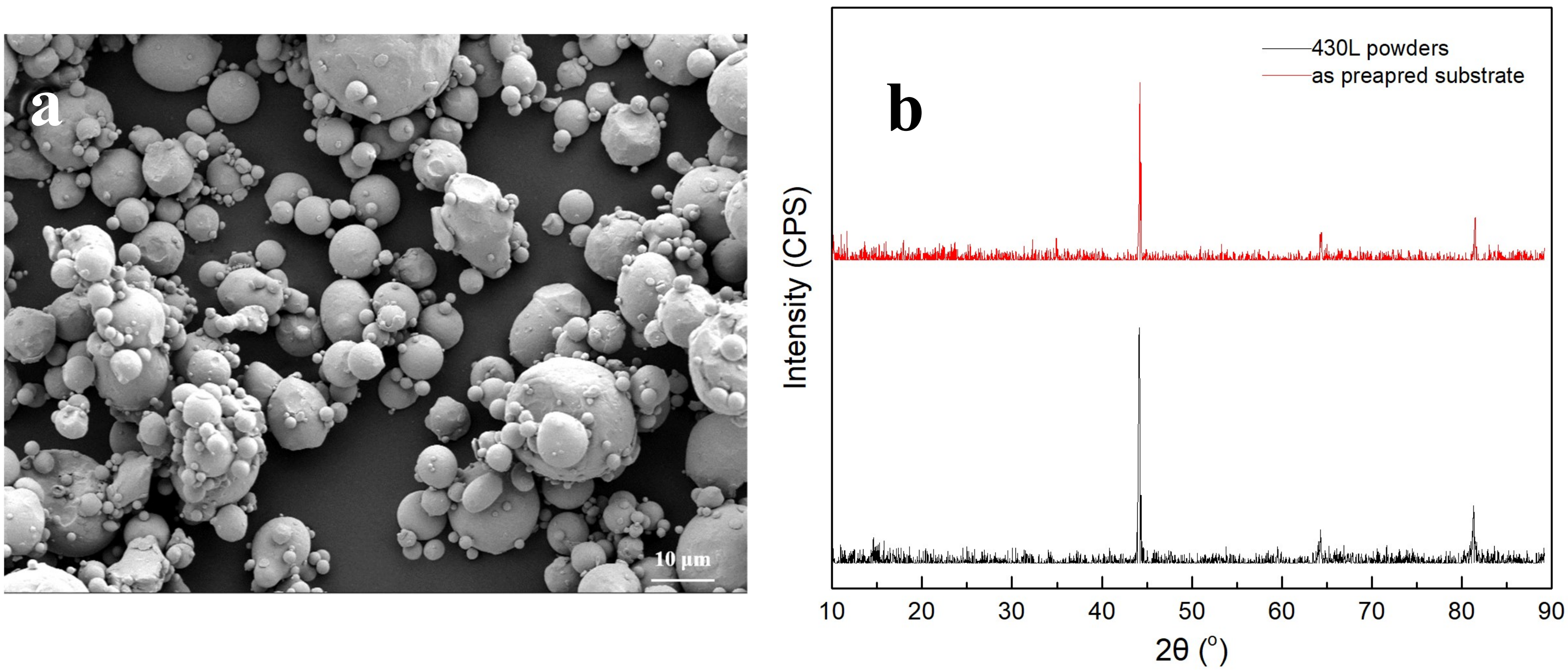

Fig.4.(a) The SEM morphology of 430L powders (D50=10 µm); (b) XRD patterns of 430L powders and as-prepared metal support after sintering.

Variation of the Metal Substrate Slurry Composition for Phase Inversion Tape Casting

❖ Composition of the casting slurry

Compositions (wt.%)				
NMP	PESf	PVP	430L	NMP:PESf:PVP
28	5.6	1.4	65	5:1:0.25
24	4.8	1.2	70	5:1:0.25
20	4	1	75	5:1:0.25
21.18	7.06	1.76	70	3:1:0.25
22.86	5.71	1.43	70	4:1:0.25
23.48	5.22	1.30	70	4.5:1:0.25
24.83	4.14	1.03	70	6:1:0.25

Effects of the Solid Loading on the Viscosity of Slurry

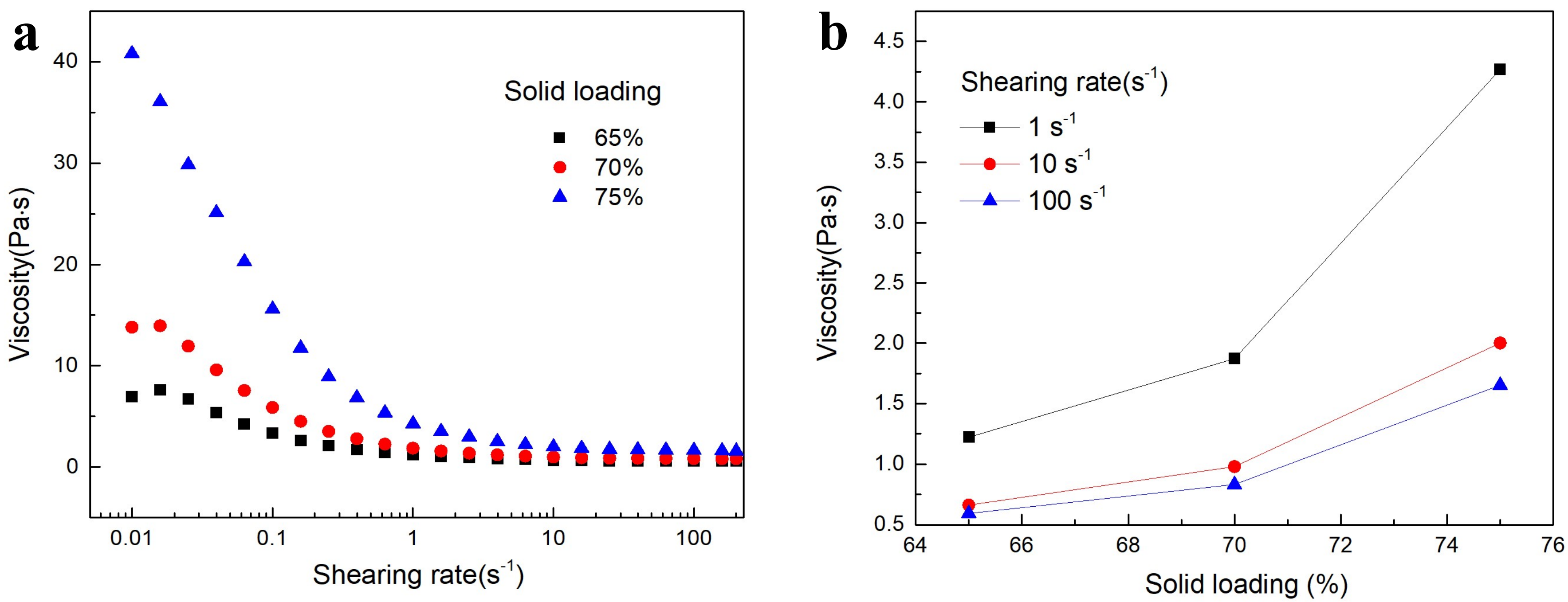

Fig.5. Rheological properties of the slurry derived from different solid loading. (a) Viscosity vs shearing rate. (b) Viscosity vs solid loading.

When the solid loading reaches a critical value (~70%), further increase in the solid loading will result in a sharp increase in the slurry viscosity

Permeability and Porosity of the Metal Substrate

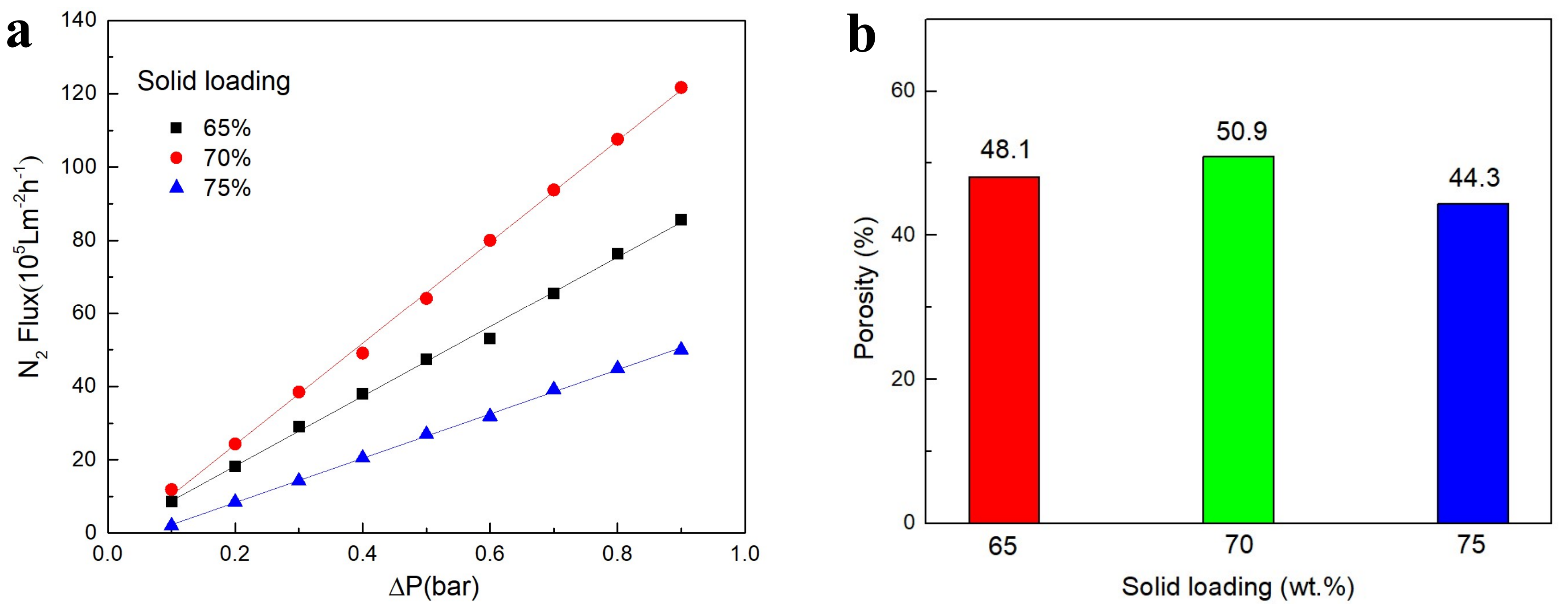

Fig.6. (a) Gas permeability and (b) porosity of the metal supports heat-treated at 520 ^oC for 1 h in air and then sintered at 1280 ^oC for 3.5 h in 5vol%H_2/95vol% N_2.

Effects of the Solid Loading on the Microstructure of the Metal Support Fabricated using Phase-Inversion Tape-Casting

❖ Cross sectional SEM of the metal support (PESf:NMP= 1:5)

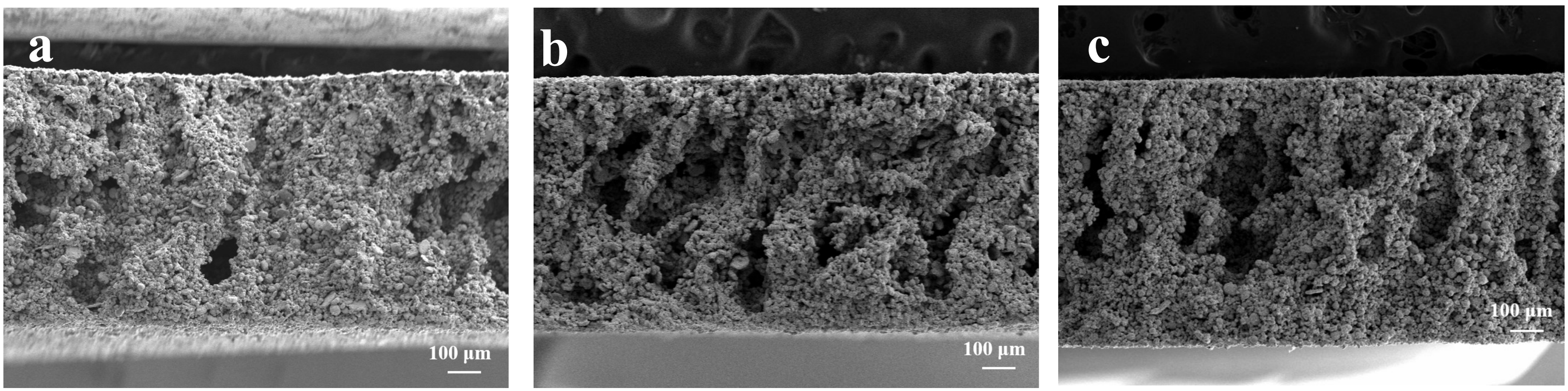

Fig.7. Cross-sectional SEM images of the as-obtained the metal supports with different metal powder loading in the slurry. (a) 65wt.%, (b) 70 wt.%, (c) 75 wt.%

The as-obtained porous metal support derived from the slurry with the solid loading of 70 wt.% has thinner sponge layer and more channels, which can improve the permeability and porosity of the corresponding metal support.

Effects of Binder Contents on the Viscosity of Slurry

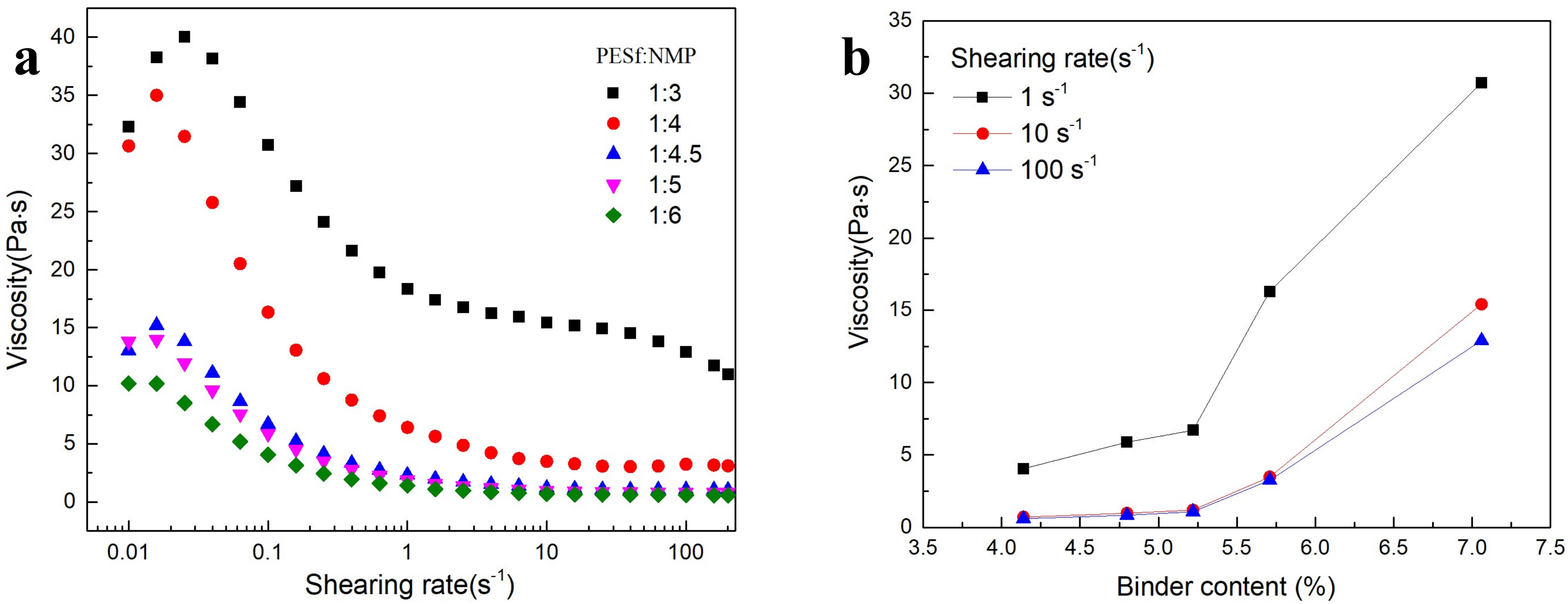

Fig.8. Rheological properties of the metal slurry derived from different binder contents. (a) Viscosity vs shearing rate. (b) Viscosity vs binder contents.

When the binder contents reach a critical value (~5.22%, PESf:NMP=1:4.5), further increase in the binder content will result in a sharp increase in the slurry viscosity

Permeability and Porosity of the Metal Support

a

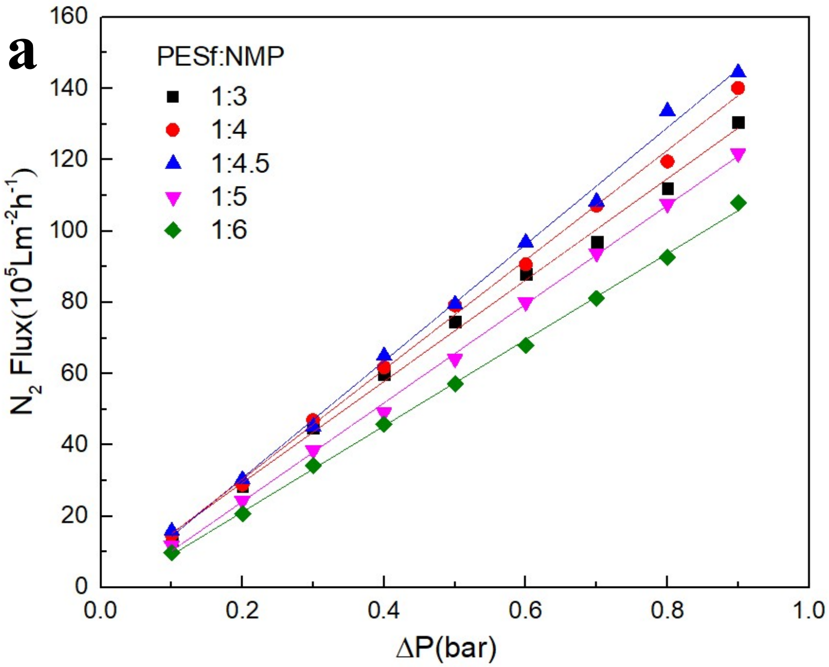

b

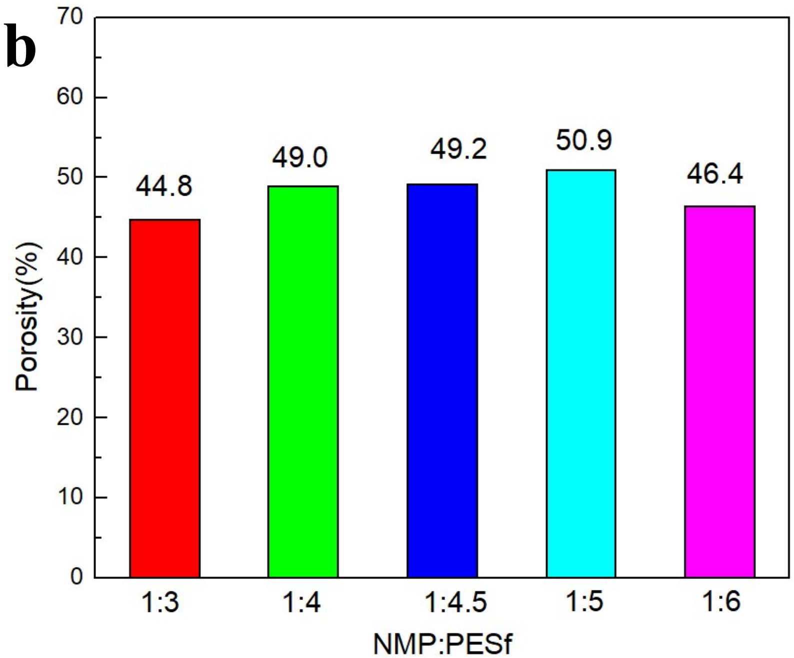

Fig.9. (a) Gas permeability and (b) porosity of the metal supports heat-treated at 520 ^{o}C for 1 h in air and then sintered at 1280 ^{o}C for 3.5 h in 5vol%H_2/95vol% N_2.

Effects of Binder Contents on the Porous Metal Support Microstructure

❖ Cross sectional SEM of metal support (70 wt.% metal powder solid loading)

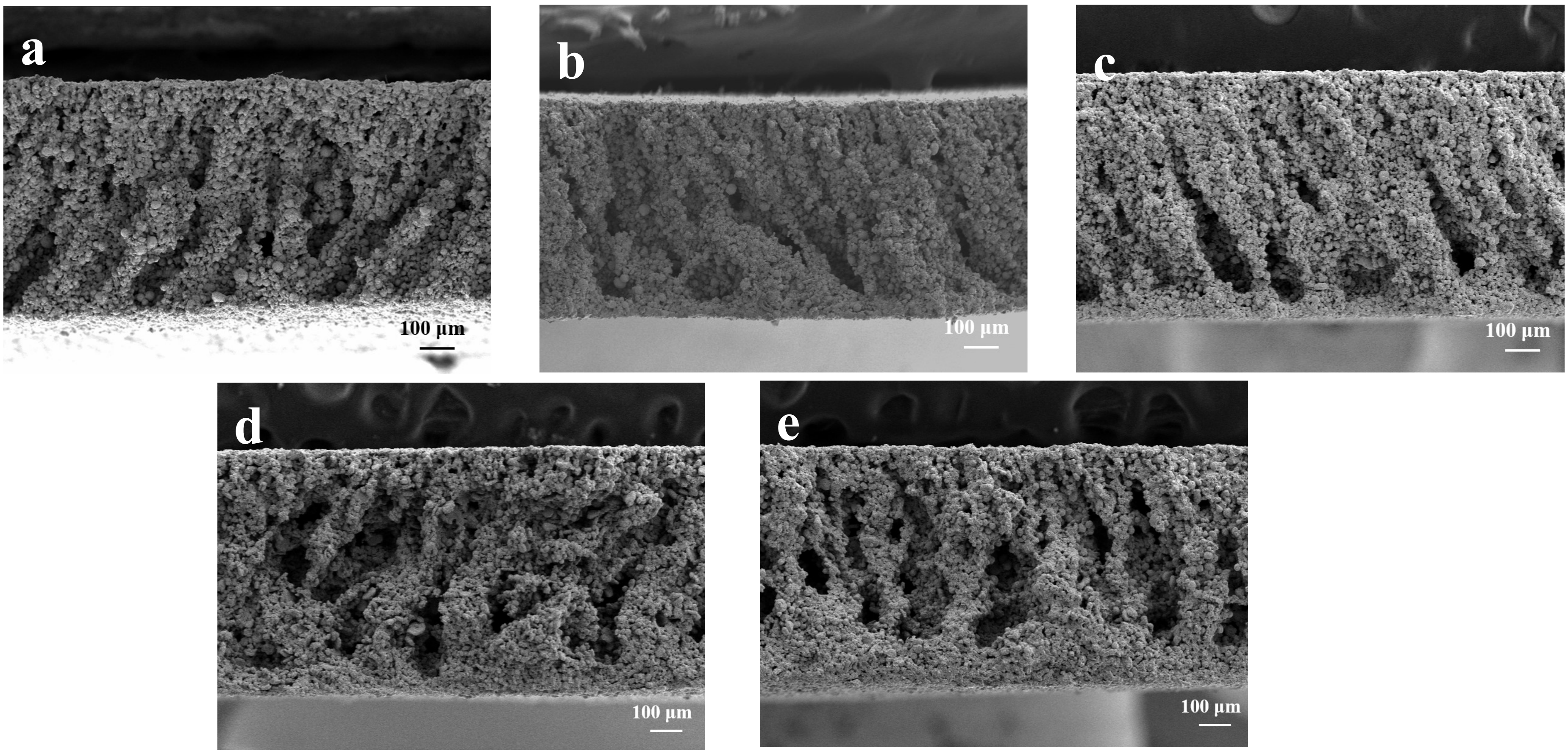

Fig.10. Cross-sectional SEM images of the as-obtained the metal supports. (a) 1:3, (b) 1:4, (c) 1:4.5, (d) 1:5, (e) 1:6.

When the ratio of PESf and NMP is 1:4.5 in the slurry, the as-prepared metal support has the desired microstructure, beneficial for the permeability and porosity.

Project Goal 2 – Fabrication of Thin-film Anode, Electrolyte and Cathode Layers using Atmospheric Plasma Spraying (APS)

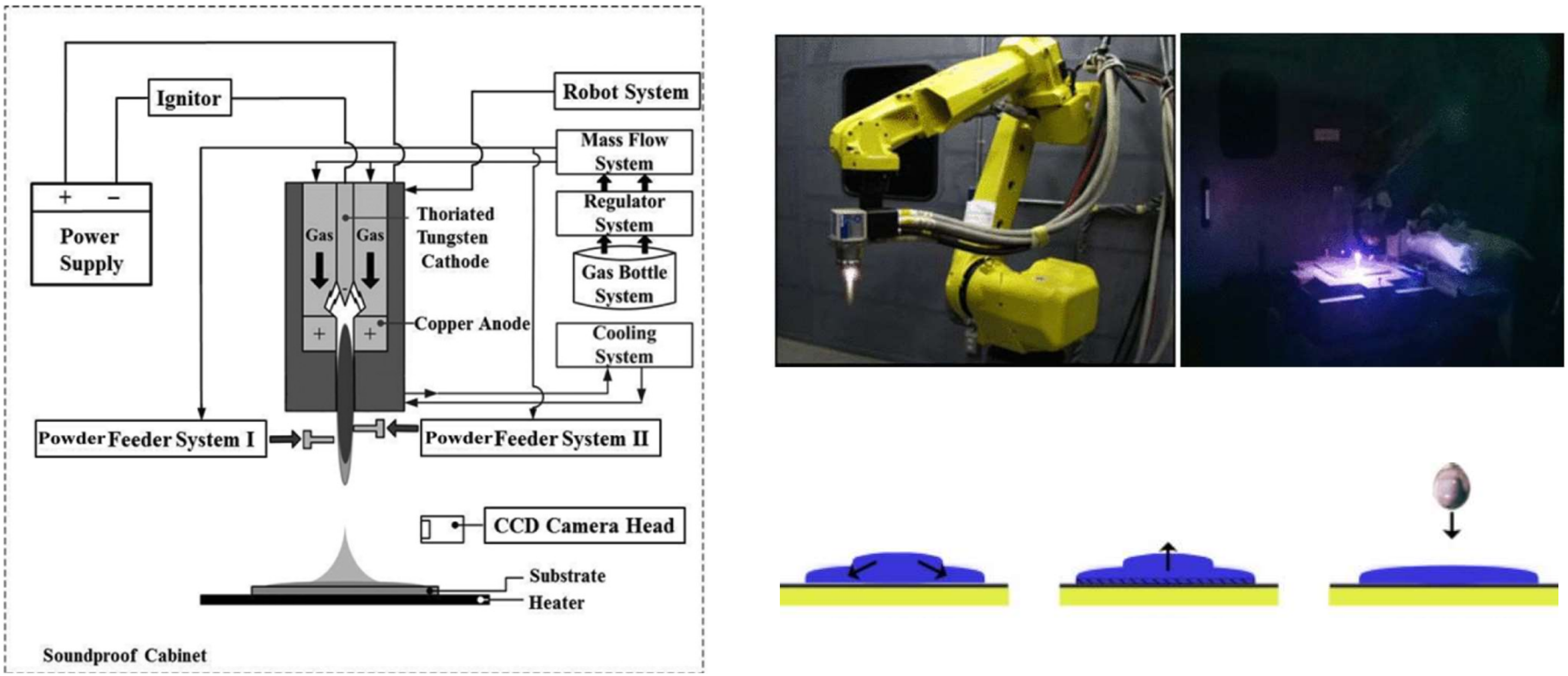

Fig.11. Schematic diagram of APS.

IEEE Transactions on Plasma Science 2016, 45(2), 318-322

Characterization of the Anode, Electrolyte and Cathode Powders for APS

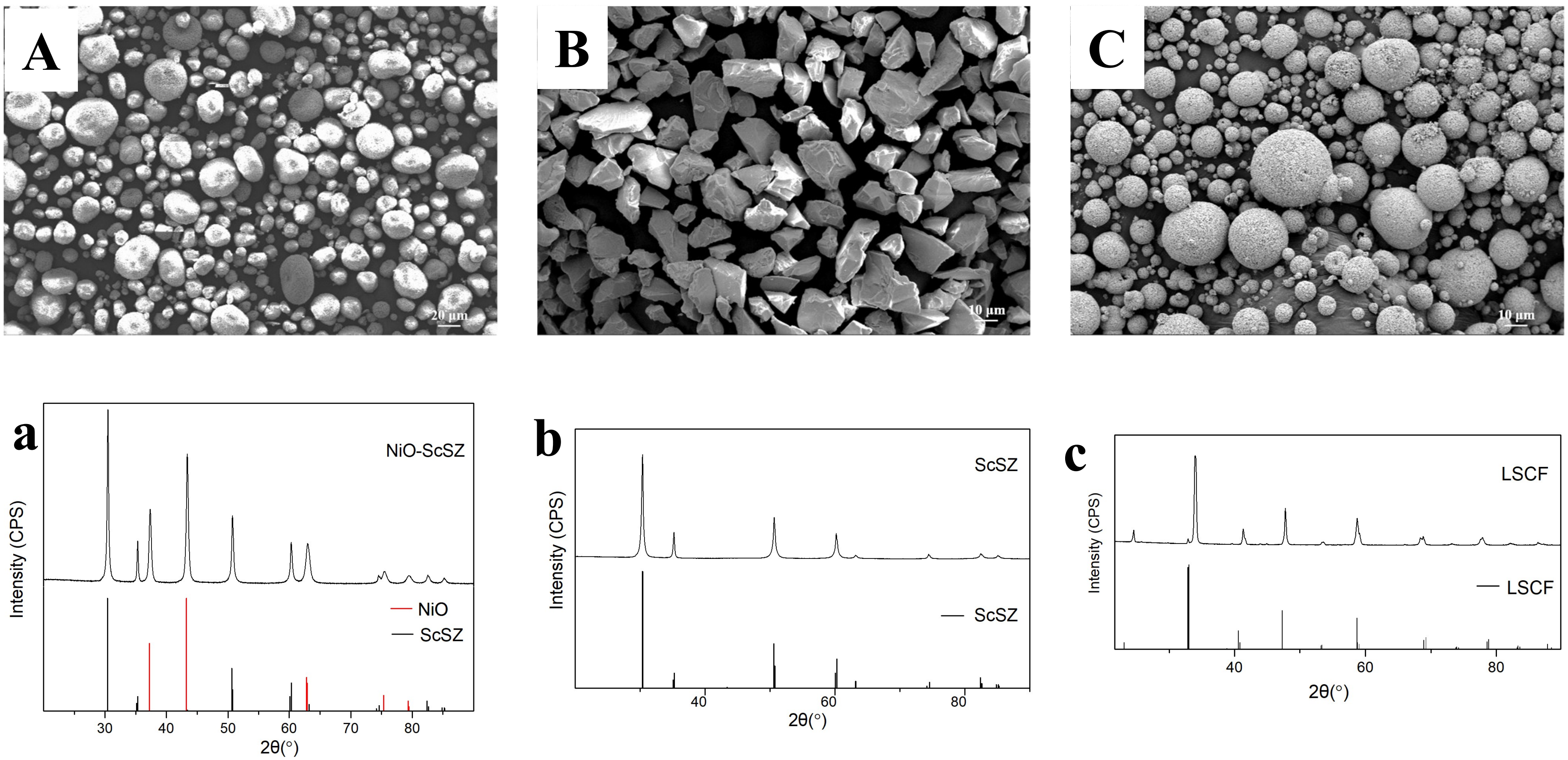

Fig.12. The SEM morphology and XRD patterns of different powders for APS. (A-a) NiO-ScSZ, (B-b) ScSZ, (C-c) LSCF.

Parameters for Deposition of the ScSZ-NiO Anode and ScSZ Electrolyte using APS

❖ Spray parameters

Parameters	NiO-ScSZ	ScSZ
Operating power (kW)	24	40
Primary gas flow rate (L min^{-1})	60	60
Secondary gas flow rate (L min^{-1})	6	6
Powder feed rate (g min^{-1})	2.5	2.5
Spraying distance (mm)	150	70/100/150
Spraying times	4	8

Effect of Spraying Distance on the Microstructure of OCV of the Half Cell

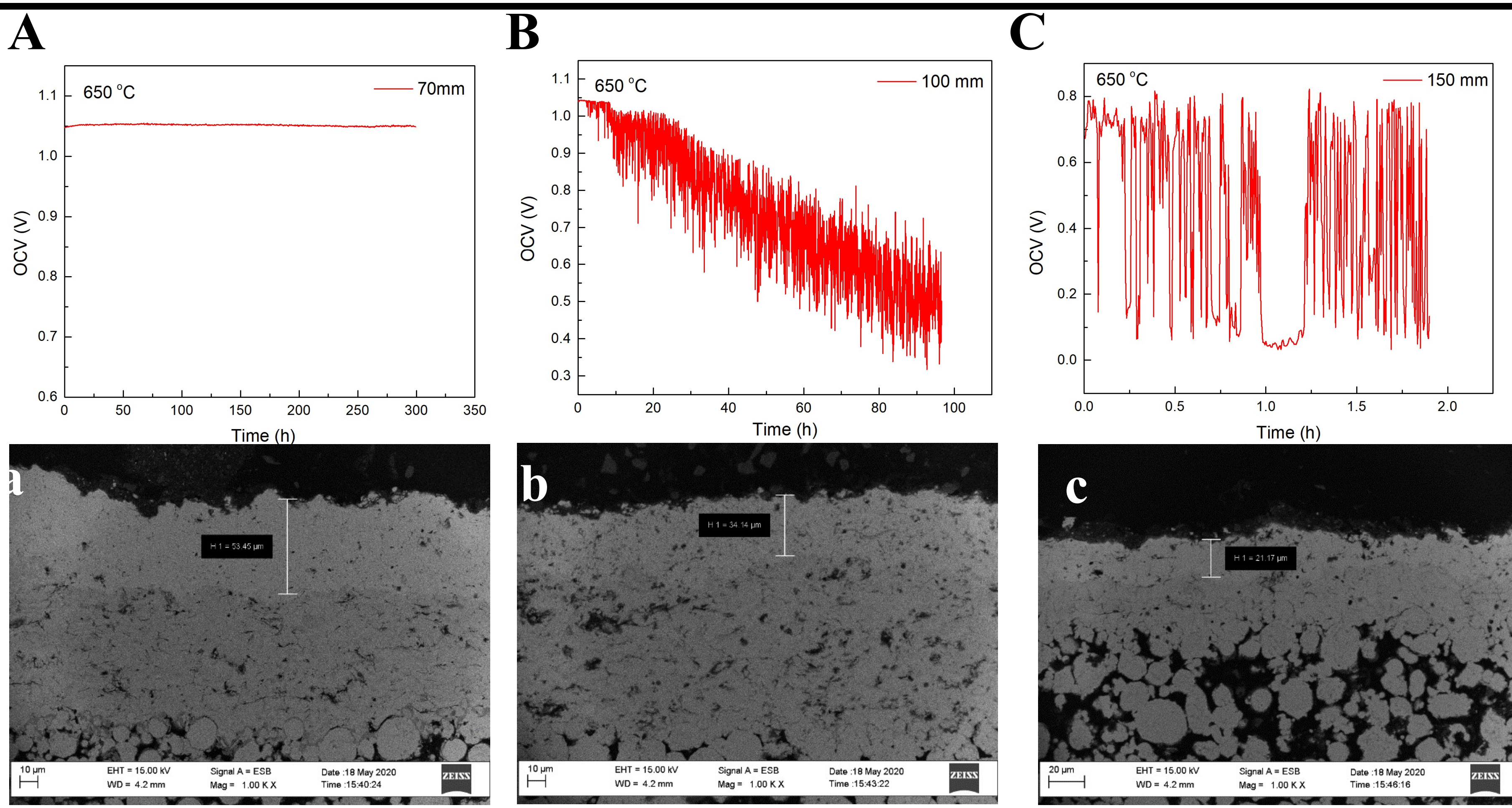

Fig.13. OCV versus time and cross-sectional SEM images for half cells with the electrolyte spraying with various distance. (A-a) 70 mm, (B-b) 100 mm, (C-c) 150 mm.

Dense ScSZ electrolyte was successfully prepared under 70 mm spraying distance

Deposition of the LSCF cathode

❖ Spray parameters

Parameters	NiO-ScSZ	ScSZ	LSCF
Operating power (kW)	24	40	6/7.5/9
Primary Argon flow rate(L min^{-1})	60	60	60
Secondary gas flow rate(L min^{-1})	6	6	6
Powder feed rate (g min^{-1})	2.5	2.5	2.5
Spraying distance (mm)	150	70	150
Spraying times	4	8	8

Effect of Operating Power to Fabricate LSCF Cathode

❖ Cross sectional SEM of MS-SOFC

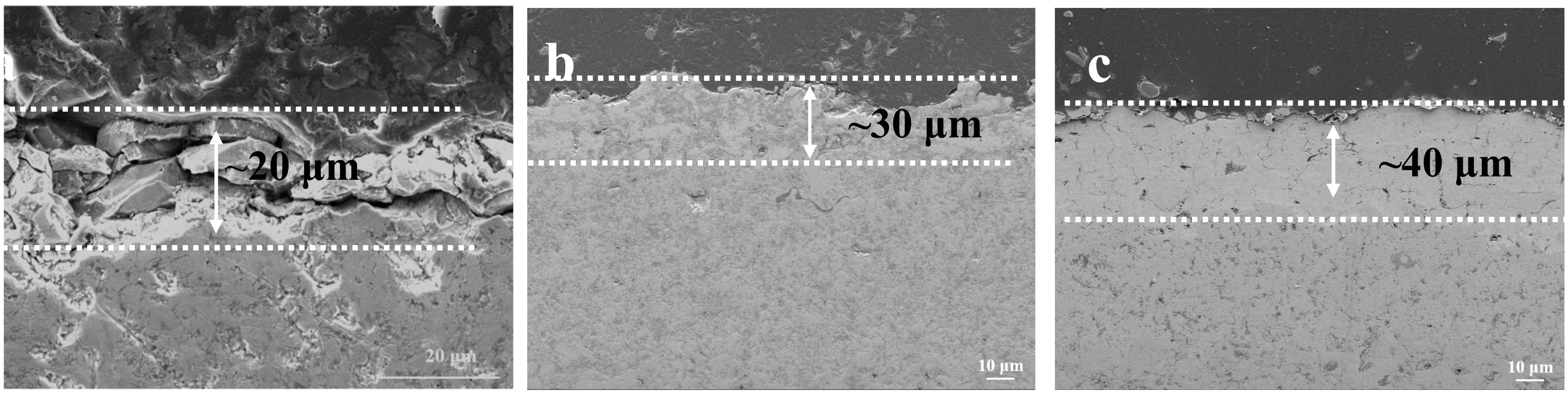

Fig.14. Cross-sectional SEM images of cathode layer for different cells. (a) 6 kW, (b) 7.5 kW, (c) 9 kW.

With improving the operating powder for depositing the cathode, the thickness of the cathode layer increases and porosity of the cathode layer decreases.

Deposition of the LSCF cathode

❖ Spray parameters

Parameters	NiO-ScSZ	ScSZ	LSCF
Operating power (kW)	24	40	6
Primary Argon flow rate(L min^{-1})	60	60	60
Secondary gas flow rate(L min^{-1})	6	6	6
Powder feed rate (g min^{-1})	2.5	2.5	2.5
Spraying distance (mm)	150	70	150
Spraying times	4	8	4/8/12

Effect of Spraying Times to Fabricate the Cathode

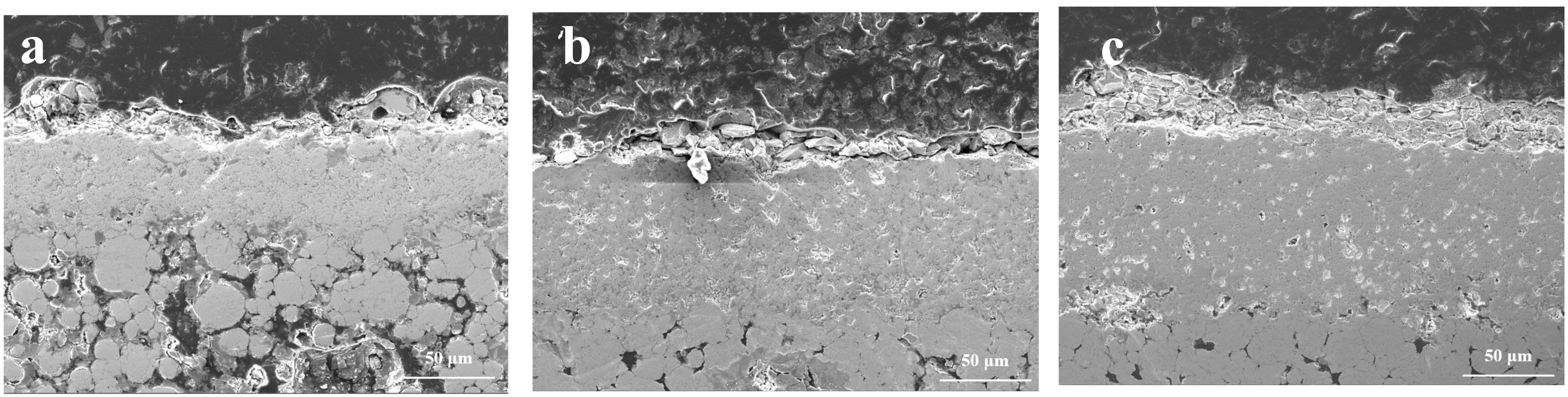

Cathode layer thickness **~12 µm** **~20 µm** **~35 µm**

Fig.15. Cross-sectional SEM images of cathode layer for different cells with the cathode fabricated with different spray times. (a) 4 times, (b) 8 times, (c) 12 times.

Increasing the number of spray times to deposit the cathode, the thickness of the cathode layer increases while the porosity of the cathode layer decreases

Project Goal 3- Characterization of the Metal-Supported SOFCs to Achieve High Performance and Stability

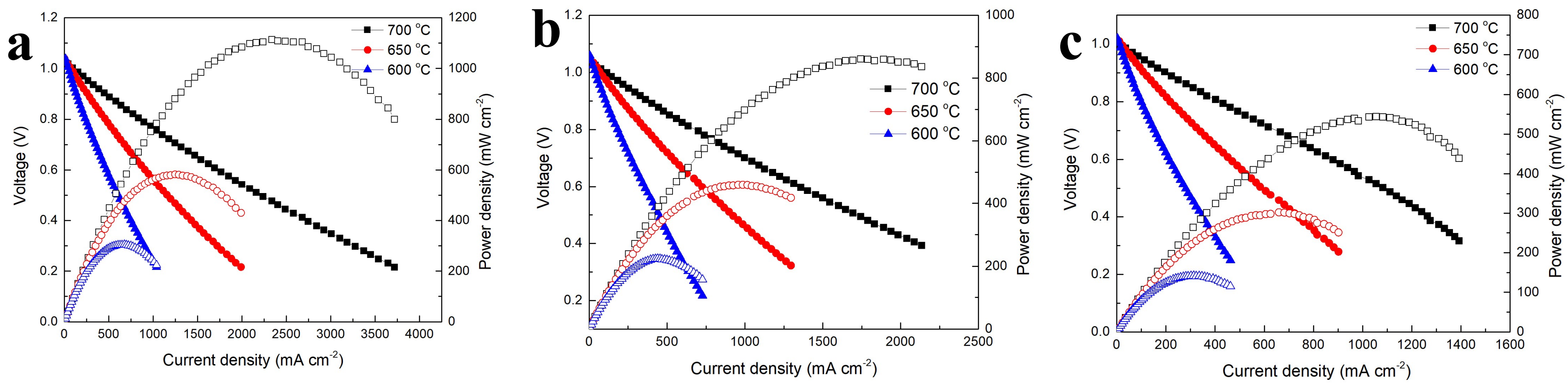

Fig.16. Current–voltage characteristics and the corresponding power densities for MS-SOFCs with LSCF cathode from different APS power. (a) 6 kW, (b) 7.5 kW, (c) 9 kW.

Table 1. OCV and maximum power density of MS-SOFCs.

T(°C)	Operating Power(kW)					
	6		7.5		9	
	OCV (V)	Pmax(mW cm^{-2})	OCV (V)	Pmax(mW cm^{-2})	OCV (V)	Pmax(mW cm^{-2})
700	1.03	1114	1.04	861	1.02	544
650	1.04	583	1.05	460	1.03	302
600	1.05	305	1.06	224	1.04	141

Effect of Operating Power to Fabricate LSCF Cathode

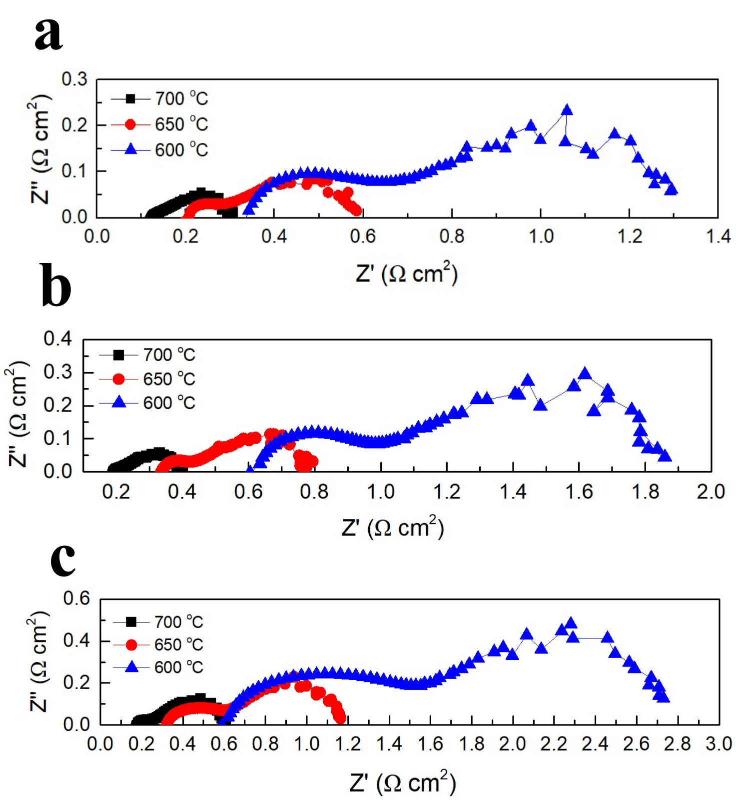

Fig.17. Impedance spectra of MS-SOFC measured from 600-700 ^{o}C. (a) 6 kW, (b) 7.5 kW, (c) 9 kW.

Table 2. Ohmic (R_{Ω}) and interfacial polarization (R_P) resistance of MS-SOFCs with cathode fabricated with different APS power.

T(^{o}C)	Operating Power(kW)					
	6		7.5		9	
	R_{Ω}(Ωcm^2)	R_P(Ωcm^2)	R_{Ω}(Ωcm^2)	R_P(Ωcm^2)	R_{Ω}(Ωcm^2)	R_P(Ωcm^2)
700	0.12	0.18	0.19	0.2	0.18	0.43
650	0.21	0.39	0.34	0.46	0.32	0.84
600	0.33	1.0	0.61	1.22	0.59	2.2

Lowering operating power can significantly enhance cell performance

Effect of Spraying Times for the Cathode on Cell Performance of the MS-SOFCs

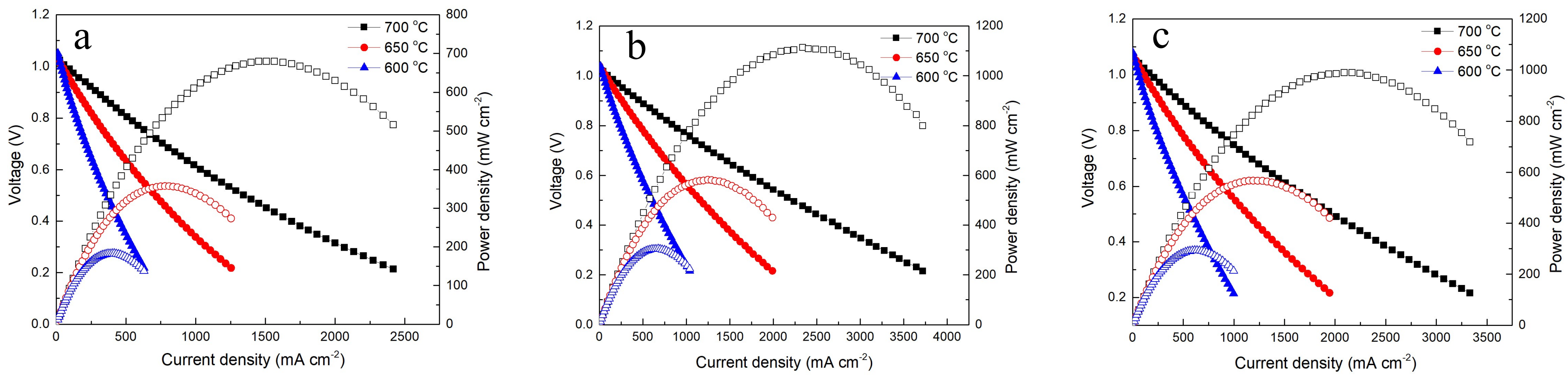

Fig.18. Current–voltage characteristics and the corresponding power densities for MS-SOFCs. (a) 4 times, (b) 8 times, (c) 12 times.

Table 3. OCV and maximum power density of MS-SOFCs.

T(°C)	Spraying times					
	4		8		12	
	OCV (V)	Pmax(mW cm^{-2})	OCV (V)	Pmax(mW cm^{-2})	OCV (V)	Pmax(mW cm^{-2})
700	1.04	680	1.03	1114	1.06	990
650	1.06	358	1.04	583	1.07	567
600	1.07	183	1.05	305	1.08	293

Effect of Spraying Times for the Cathode on Cell Performance of the MS-SOFCs

a

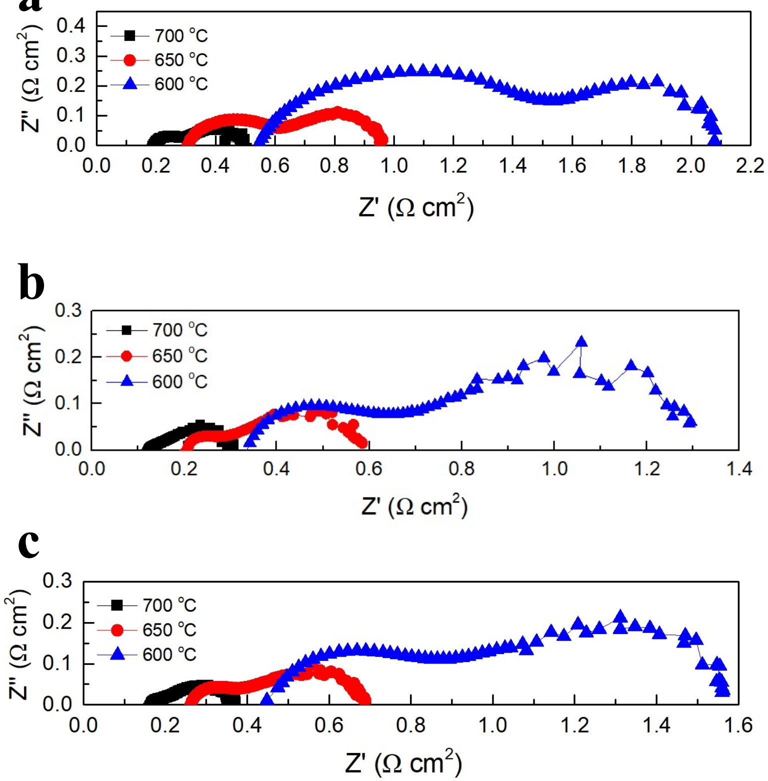

Fig.19. Impedance spectra of MS-SOFC measured from 600-700 °C. (a) 4 times, (b) 8 times, (c) 12 times.

Table 4. Ohmic(R_Ω) and interfacial polarization (R_P) resistance of various MS-SOFC.

T(°C)	Spraying times					
	4		8		12	
	R_Ω(Ωcm^2)	R_P(Ωcm^2)	R_Ω(Ωcm^2)	R_P(Ωcm^2)	R_Ω(Ωcm^2)	R_P(Ωcm^2)
700	0.19	0.30	0.12	0.18	0.16	0.2
650	0.31	0.65	0.21	0.39	0.26	0.43
600	0.55	1.53	0.33	1.0	0.44	1.14

Interface resistance significantly decreases when the spraying of 8 times is used to fabricate the cathode

Summary

- Porous metal support with open channel porous microstructures and graded porosity has been obtained using phase inversion tape casting method.

- Thin film anode, electrolyte and cathode has been successfully deposited on porous metal support using the APS process.

- Optimizing the parameters of APS can significantly enhance the electrochemical performance of MS-SOFCs.

Ongoing and Future Work

- **Optimize the processing parameters to improve the cell performance.**

- **Evaluate the performance stability of MS-SOFCs.**

- **Fabricate and characterize large size MS-SOFCs.**

Acknowledgements

- The financial support from the U.S. Department of Energy, Office of Fossil Energy (DE-FE0031670) is gratefully acknowledged.

- We thank Dr. Patcharin Burke, Dr. Venkat Venkataraman, Dr. Shailesh Vora, as well as the entire NETL SOFC team for guidance of this work.